A novel ruthenium(II) complex for two-photon absorption-based optical power limiting in the near-IR range†

Mickaël Four,[a] Didier Riehl,[b] Olivier Mongin,[c] Mireille Blanchard-Desce,[c] Latévi Max Lawson-Daku,[d] Juliette Moreau,[g] Jérôme Chauvin,[e] Jacques A. Delaire[f] and Gilles Lemercier*[g]

In this article, the synthesis of a novel high-conjugated ligand and its corresponding Ru(II) complex **PTFTF:Ru** is reported, along with the linear and nonlinear optical characterizations. Two-photon absorption based optical power limiting properties (OPL), especially in the near infrared, are described and compared to those of the analogous complexes previously published. Combined with a preliminary theoretical approach, this allows us to highlight several key parameters for OPL optimization in such molecular systems and more particularly the spectral overlap between TPA and excited-state absorption.

I. Introduction

Optical power limiting (OPL) aims at protecting detectors (optical sensors and human eyes) from high-power pulsed lasers. Given the rapid development of such lasers, there is a vivid interest in the design of efficient optical limiters. These systems exhibit a high constant transmission at low incident fluences, but a high extinction at incident fluences greater than the OPL threshold.[1] Different nonlinear processes can lead to efficient extinction by decreasing the OPL threshold: nonlinear scattering,[2,3] reverse saturable absorption,[4–6] nonlinear refraction[7] and two-photon absorption (TPA).[8–12] This last process presents several advantages such as (*i*) high transmission at low laser intensity (one- and two-photon absorption usually do not overlap), (*ii*) no saturation effect and (*iii*) an instantaneous response time. In the nanosecond pulse range and following TPA process, an excited state absorption (ESA) can occur at the same excitation wavelength

and participate to the increase of the efficiency in the OPL properties. The OPL therefore results from a [2 + 1] photon process during the pulse. Although ESA could be observed from singlet states of organic molecules,[13] excited states with longer lifetimes, as shown for metallic complexes such as platinum(II) compounds,[14,15] should favour this phenomenon.

In this context, Ru(II) complexes are of great interest due to the long-lived metal-to-ligand charge-transfer (^{3}MLCT) excited state. Moreover, octupolar coordination Ru(II) complexes were reported, displaying moderate to high TPA efficiency.[16–20] Despite these interesting properties, only a few Ru(II) complexes have been studied for their OPL efficiency.[21–23] Recently, we reported the design of novel bifluorene-substituted 1,10-phenanthroline based Ru(II) coordination complexes for TPA and OPL in the near-IR range, related to their long-lived ^{3}MLCT excited state (around the microsecond).[24] The TPA and ESA properties of these compounds were found to be strongly dependent on the π-conjugated ligands, bearing one or two fluorene moieties as TPA chromophores. Aiming to complete the structure-properties relationship, we report here the synthesis of a novel high-conjugated ligand and its corresponding Ru(II) complex **PTFTF:Ru** (see Fig. 1), along with the linear and nonlinear optical characterizations. Optical power limiting properties, and especially in the near infrared, are described and compared to those of the analogous complexes previously reported. This allows us to highlight the key parameters for OPL optimization in such molecular systems.[24]

II. Experimental section

Synthesis

^{1}H and ^{13}C NMR spectra were recorded on a Bruker DPX 200 spectrometer (at 200.13 MHz for ^{1}H and 50.32 MHz for ^{13}C)

[a] Université de Lyon, UMR CNRS n°5182, Laboratoire de Chimie École Normale Supérieure de Lyon-46, allée d'Italie, 69364 Lyon cedex 07, France
[b] Centre d'Expertise Parisien, Délégation Générale pour l'Armement (DGA), 16, bis avenue Prieur de la Côte d'Or, 94114 Arcueil, France
[c] Université Rennes 1, UMR CNRS 6510, Chimie et Photonique Moléculaires, Campus de Beaulieu, 35042 Rennes cedex, France
[d] Facultés des Sciences-Université de Genève, 30 quai Ernest Ansermet, CH-1211 Genève 4, Suisse
[e] Université Joseph Fourier, CNRS 5250, ICMG FR-2607, Département de Chimie Moléculaire, B.P. 5, 38402 St Martin d'Hères, France
[f] Laboratoire de Photophysique et Photochimie Supramoléculaires et Macromoléculaires, UMR 8531 CNRS Ecole Normale Supérieure de Cachan 61, Avenue du Président Wilson, 94235 Cachan cedex, France
[g] Université de Reims Champagne-Ardenne, ICMR UMR CNRS n° 6229-C^{2}POM Team, BP 1039-51687, Reims cedex 2, France. E-mail: gilles.lemercier@univ-reims.fr
† Electronic supplementary information (ESI) available: See DOI: 10.1039/c1cp21661a
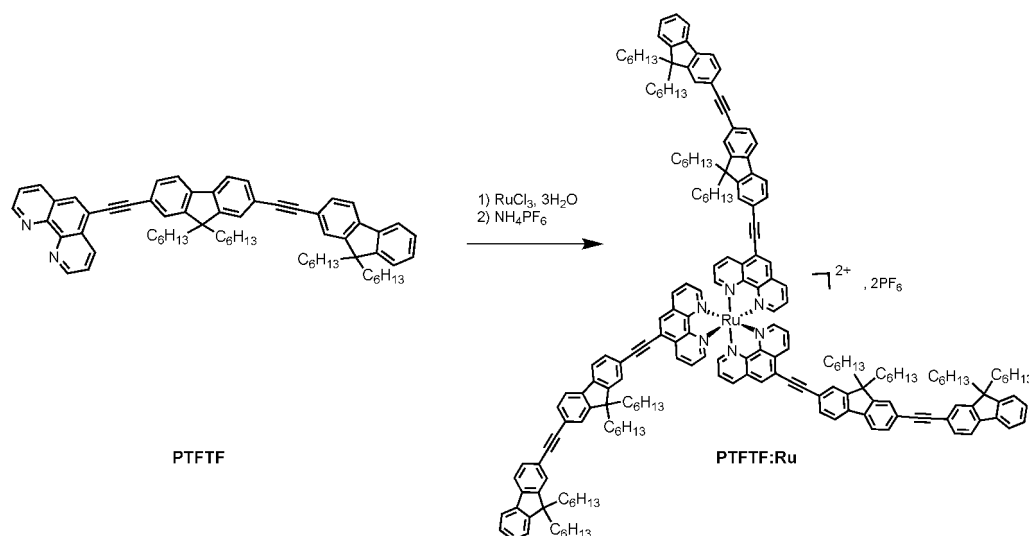
Fig. 1 Molecular structures of the **PTFTF** ligand and the **PTFTF:Ru** complex.

and also on a Varian Unity Plus at 499.84 MHz for ^{1}H. Elemental analyses were carried out by the "*Service Central d'Analyse*", CNRS. UV/Vis spectra were recorded in the 200–800 nm range on a UV/Vis Jasco V-550; λ_{max} are given in nm and molar extinction coefficients ε in L.mol^{-1}.cm^{-1}. Synthesis and characterizations of compounds **1**,[25] and **2**[26] have already been described elsewhere (see Fig. 2, for the compound number).

Compound 3

In a 100 mL round bottom flask, 1.15 g of 2-bromo-7-iodo-9,9-dihexylfluorene **2** (2.13 mmol, 1.1 eq.), 41 mg CuI (0.21 mmol, 0.11 eq.) and 136 mg of dichlorobis(triphenylphosphine)-palladium(II) (0.19 mmol, 0.1 eq.) were dissolved under argon in 10 mL of distilled THF and 20 mL of triethylamine. 10 mL of a solution of 2-ethynyl-9,9-dihexylfluorene (689 mg, 1.94 mmol, 1 eq.). Compound **1** in distilled THF was then added and the solution was stirred for one night. After cooling to room temperature, the reaction mixture was dropped in 50 mL of a saturated solution of NH$_4$Cl. The aqueous layer was extracted with diethyl ether (2 × 20 mL). Organic phases, were washed with saturated solution of ammonium chloride (2 × 20 mL), 20 mL of a saturated solution of NaCl, before to be dried over

anhydrous Na$_2$SO$_4$. After evaporation of the solvent, the brownish oil obtained was purified by chromatography on silica (pentane then pentane : dichloromethane 90 : 10) to give 1.02 g of a yellow powder (68% yield). ^{1}H NMR (200.13 MHz; CDCl$_3$): δ (ppm) 7.71–7.64 (m, 3H); 7.58–7.45 (m, 7H); 7.36–7.33 (m, 3H); 2.05–1.90 (m, 8H); 1.20–0.9 (m, 24H); 0.82–0.73 (m, 12H); 0.70–0.50 (m, 8H); ^{13}C-NMR (50.32 MHz; CDCl$_3$): δ (ppm) 153.39; 151.16; 150.95; 150.57; 141.62; 140.58; 140.34; 139.66; 130.91; 130.74; 130.25; 127.67; 127.03; 126.33; 126.06; 123.03; 122.30; 121.66; 121.55; 121.46; 120.13; 119.91; 119.81. IR (KBr): σ(cm^{-1}): 3055; 2952; 2927; 2856; 1456; 811; 739. Anal. Calcd. for C$_{52}$H$_{65}$Br (769.98 g mol^{-1}) Calcd (%): C. 81.11 H 8.51; Found (%): C 81.87. H 8.55.

Compound 4: TMS-protected intermediate

970 mg of 2-bromo-7-(2-(9,9-dihexylfluoren-2-yl)-ethynyl)-9,9-dihexylfluorene **3** (1.26 mmol, 1 eq.), 26 mg CuI (1.39 mmol, 0.11 eq.) and 88 mg of dichlorobis(triphenylphosphine)-palladium(II) (0.13 mmol, 0.1 eq.) were dissolved under argon in a mixture of 15 mL of distilled THF and 15 mL triethylamine. Then, 0.89 mL of ethynyltrimethylsilane (60.30 mmol, 5 eq.) was added and the reaction mixture stirred for the night at
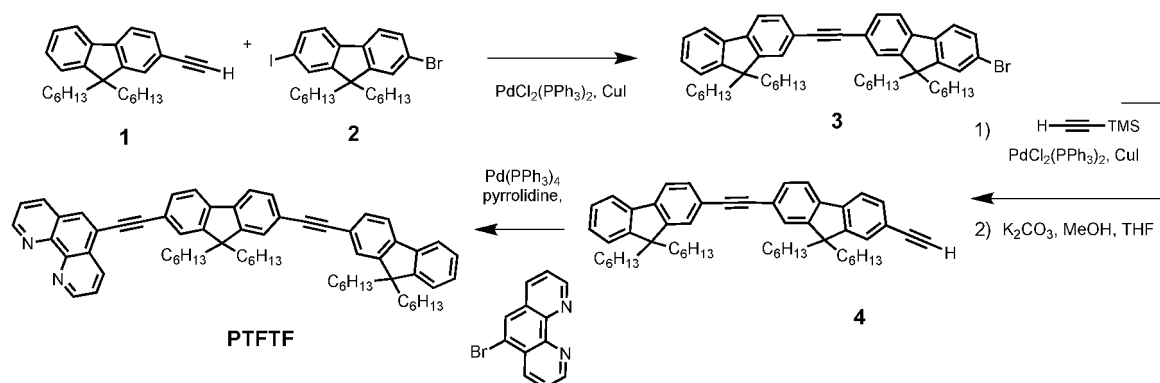

Fig. 2 Synthesis of the **PTFTF** ligand.

70 °C in a closed schlenk. The resulting solution was dropped at room temperature in 20 mL of a NH_4Cl saturated solution and 20 mL of diethyl ether were added. Aqueous phase was extracted three times with 20 mL diethyl ether and the resulting organic layers, were washed twice with a saturated solution NH_4Cl (2×20 mL) and 20 mL of a saturated solution of NaCl before to be dried over Na_2SO_4. The resulting brownish oil obtained after evaporation of the solvent was purified using column chromatography on silica (petroleum ether : dichloromethane from 100 : 0 to 90 : 10) to give a yellow solid (875 mg, 88% yield). ^{1}H-NMR (200.13 MHz; $CDCl_3$): δ (ppm) 7.72–7.45 (m, 10H); 7.36–7.33 (m, 3H); 2.05–1.92 (m, 8H); 1.20–0.95 (m, 24H); 0.82–0.74 (m, 12H); 0.70–0.50 (m, 8H); 0.30 (s, 9H); ^{13}C-NMR (50.32 MHz; $CDCl_3$): δ (ppm) 151.27; 151.16; 151.07; 150.94; 141.60; 141.11; 140.68; 140.58; 131.41; 130.84; 130.74; 127.66; 127.03; 126.38; 126.07; 123.01; 122.32; 121.85; 121.58; 120.13; 119.92; 119.81; 106.29; 94.40; 91.09; 90.52; 55.39; 55.29; 40.62; 31.73; 31.69; 29.88; 23.87; 22.79; 22.75; 14.14; 0.21. IR (KBr): $\sigma(cm^{-1})$: 3060; 2954; 2927; 2856; 2154 ($C{\equiv}C$); 1466; 1250; 887; 845; 822; 739. Anal. Calcd. for $C_{57}H_{74}Si$ (787.28 g mol^{-1}) (%): C 86.96. H 9.47; Found (%): C 86.91. H 9.35. **Deprotection step**: 875 mg of the TMS intermediate (1.11 mmol, 1 eq.) and 307 mg K_2CO_3 (2.22 mmol, 2.2 eq.) were dissolved in distilled THF and 20 mL methanol. The reaction mixture was stirred for 2 h at room temperature. 20 mL H_2O and 20 mL diethyl ether were added, and the aqueous phase was extracted three times by ethyl ether (3×20 mL). Organic layers were washed twice with water (2×20 mL), 20 mL of a saturated NaCl solution, then dried over anhydrous Na_2SO_4. After evaporation of the solvent, the resulting brownish oil was purified using column chromatography on silica (petroleum ether:dichloromethane from 100 : 0 to 95 : 5) to give **4** as a yellow solid (729 mg, 92%).-^{1}H NMR (200.13 MHz; $CDCl_3$): δ (ppm) 7.72–7.67 (m, 4H); 7.63–7.48 (m, 6H); 7.35–7.32 (m, 6H); 3.16 (s, 1H). 2.03–1.94 (m, 8H); 1.20–0.97 (m, 24H); 0.82–0.73 (m, 12H); 0.70–0.50 (m, 8H); ^{13}C NMR (50.32 MHz; $CDCl_3$): δ (ppm) 151.29; 151.17; 150.95; 141.63; 141.39; 140.58; 131.41; 130.87; 130.75; 127.67; 127.03; 126.67; 126.08; 123.03; 122.45; 121.55; 120.78; 120.22; 120.14; 120.02; 119.08; 91.12; 90.45; 84.78; 77.41; 55.39; 55.30; 40.61; 31.69; 29.88; 23.87; 22.76; 14.14. IR (KBr): $\sigma(cm^{-1})$: 3305 ($C{\equiv}C{-}H$); 3060; 2952; 2927; 2854; 2206 ($C{\equiv}C$); 1466; 891; 822; 739. Anal. Calcd. for $C_{54}H_{66}$ (715.10 g mol^{-1}) Calc (%): C 90.70 H 9.30 Found (%): C 90.55. H 9.40.

PTFTF

2-ethynyl-7-(2-(9,9-dihexylfluoren-2-yl)ethynyl)-9,9-dihexylfluorene **4** (302 mg, 0.42 mmol, 1.1 eq.) and 99 mg of 5-bromo-1,10-phenanthroline **1** (0.38 mmol, 1 eq.) were dissolved in 20 mL pyrrolidine under argon. Then, 67 mg of tetrakis(triphenylphosphine)palladium(0) (0.058 mmol, 0.15 eq.) were added and the reaction mixture was stirred for 18 h at 70 °C before to be cooled to room temperature and dropped in 30 mL of a saturated NH_4Cl solution. Aqueous layer was extracted three times with 30 mL dichloromethane. The organic phases were washed successively with a saturated solution of ammonium chloride (2×30 mL) and a saturated solution of NaCl (30 mL), then dried on anhydrous sodium sulfate. After evaporation of

the solvent, brownish oil was purified on alumina column (dichloromethane : petroleum ether : triethylamine–from 80 : 20 : 1 to 100 : 0 : 1) to give an orange oil. Recristallization in hot acetonitrile gave 225 mg of the desired ligand as a yellow solid (66% yield). ^{1}H NMR (200.13 MHz; $CDCl_3$): δ (ppm) 9.26 (dd. 1 H, ^3J = 4.3 Hz. ^4J = 1.7 Hz); 9.20 (dd. 1 H, ^3J = 4.3 Hz, ^4J = 1.7 Hz); 8.91 (dd. 1 H, ^3J = 8.2 Hz, ^4J = 1.7 Hz); 8.24 (dd. 1 H, ^3J = 8.2 Hz, ^4J = 1.7 Hz); 8.14 (s, 1H); 7.81–7.55 (m, 12 H); 7.34–7.32 (m, 3H); 2.09–1.95 (m, 8 H); 1.10–1.00 (m, 24H); 0.80–0.73 (m, 12H); 0.67–0.52 (m, 8H); ^{13}C NMR (50.32 MHz; $CDCl_3$): δ (ppm) 151.48; 151.30; 151.15; 151.03; 151.95; 150.95; 150.85; 146.29; 146.17; 141.66; 140.54; 140.49; 135.90; 137.99; 131.18; 130.95; 130.73; 128.46; 128.29; 127.68; 127.02; 126.15; 126.11; 126.06; 123.64; 123.53; 123.02; 122.62; 121.49; 121.29; 120.30; 120.13; 119.81; 96.67; 91.27; 90.42; 86.36; 55.51; 55.29; 40.61; 31.72; 31.67; 29.87; 23.87; 22.76; 22.74; 14.14. IR (KBr): $\sigma(cm^{-1})$: 3060; 3033; 2953; 2926; 2854; 2200 ($C{\equiv}C$); 1468; 1421; 891; 822; 739. Anal. Calcd. for $C_{66}H_{72}N_2$. $2H_2O$ (929.32 g mol^{-1}) (%): C 85.30; H 8.24; N 3.01; Exp (%): C 85.43. H 8.01. N 3.11.

PTFTF:Ru

5 mL of an anhydrous DMF solution of 175 mg compound **PTFTF** (0.20 mmol, 3.05 eq) was dropwise added under argon, to 16.8 mg of $RuCl_3$, $3H_2O$ (0.06 mmol) also dissolved in DMF and then refluxed for a night. Saturated aqueous solution of NH_4PF_6 was added to the resulting solution at room temperature. The precipitate was collected by filtration, washed three times with H_2O and twice with pentane. The filtration and evaporation gave 147 mg of a red-brownish solid with 75% yield. m.p.: not found (20–450 °C). ^{1}H NMR (499.84 MHz, $CDCl_3$) δ (ppm) 8.95–8.94 (m, 1H); 8.62–8.48 (m, 2H); 8.36–8.35 (m, 1H); 8.30–8.29 (m, 1H); 8.09–8.02 (m, 2H); 7.76–7.63 (m, 6H); 7.58–7.53 (m, 4H); 7.34–7.31 (m, 3H); 2.05–1.95 (m, 8H, H_{alkyl}); 1.12–1.03 (m, 24H, H_{alkyl}); 0.78–0.75 (m, 12H, H_{alkyl}); 0.64–0.60 (m, 8H, H_{alkyl}). UV/Vis ($CHCl_3$): λ_{max} (ε) = 450 (47 610); 401 (114 510); 341 (143 020); 273 (97 700); 231 (138 550). IR (KBr, cm^{-1}): 3060–3448 ($\nu_{O\text{-}H}$, H_2O); 2930 ($\nu C\text{-}H_{alkyl}$); 2850 ($\nu C\text{-}H_{alkyl}$); 2200 ($\nu C{\equiv}C$); 1468 ($\nu C{=}C_{aro}$); 1450 ($\nu C{=}C_{aro}$); 1420 ($\nu C{=}C_{aro}$); 739 ($\nu C\text{-}H_{aro}$). Anal. Calcd. for $RuC_{198}H_{216}N_6P_2F_{12}$, 5 H_2O: C, 75.23; H, 7.21; N, 2.66; Ru, 3.20. Found: C, 75.00; H, 7.16; N, 2.91; Ru, 3.16%. ESI-HRMS Calcd for Ru $C_{198}H_{216}N_6P_2F_{12}$: 2779.6130 M$^+$, exp: 2779.6312.

Luminescence

The steady-state emission spectra were recorded on a Photon Technology International (PTI) SE-900M spectrofluorimeter. All the samples were prepared in a glove box using deoxygenated CH_3CN. The samples were put in 1 cm quartz cell and maintained in anaerobic conditions with a Teflon cap. Emission quantum yields ϕ_L were determined at 25 °C in deoxygenated acetonitrile solutions using a CH_3CN solution of $[Ru^{II}(Phen)_3](PF_6)_2$ (ϕ_L^{ref} = 0.03) as a standard, according to eqn (1)

$$\phi_L^S = \frac{I_L^S}{I_L^{Ref}} \frac{(1 - 10^{-OD^{Ref}})}{(1 - 10^{-OD^S})} \phi_L^{Ref} \qquad (1)$$

where I_L, the emission intensity, was calculated from the area of the emission band $\int I(\lambda)d\lambda$, OD represents the optical density at the excitation wavelength. The superscripts "S" and "Ref" refer to the sample and the standard, respectively. The luminescence lifetime of the Ru(II) complexe was determined after irradiation of the sample at $\lambda = 337$ nm with a 4 ns pulsed N$_2$ laser (Optilas VSL-337ND-S), from the record of the emission signal at the emission maximum wavelength using a monochromator and a photomultiplier tube (Hamamatsu R928) coupled with an ultra-fast oscilloscope (Tektronix TDS 520A).

Two-photon absorption

The two-photon absorption spectra of the complexes and the ligands were determined in the 700–930 nm range by investigating their two-photon excited luminescence (TPEL) in deoxygenated 10^{-4} mol L^{-1} acetonitrile or dichloromethane solutions. The measurements were performed using a Nd:YLF-pumped Ti:sapphire oscillator generating 150 fs pulses at a 76 MHz rate. The excitation was focused into the cuvette through a microscope objective (10×, NA 0.25). The luminescence was detected in epifluorescence mode via a dichroic mirror (Chroma 675dcxru) and a barrier filter (Chroma e650sp-2p) by a compact CCD spectrometer module BWTek BTC112E. Total luminescence intensities were obtained by integrating the corrected emission spectra measured by this spectrometer. TPA cross-sections (σ_{TPA}) were determined from the two-photon excited luminescence cross-sections ($\sigma_{TPA}\Phi$) and the luminescence emission quantum yield (Φ). TPEL cross-sections of 10^{-4} M solutions were measured relative to a 10^{-4} M solution of fluorescein in 0.01 M aqueous NaOH for 715–930 nm, using the well-established method described by Xu and Webb[27] and the appropriate solvent-related refractive index corrections.[28] Data points between 700 and 715 nm were corrected according to ref. 29. The quadratic dependence of the luminescence intensity on the excitation power was checked for each sample and all wavelengths, indicating that the measurements were carried out in intensity regimes where saturation or photodegradation did not occur.

The experimental setup for **ESA measurements** has been described elsewhere.[30] We used a Q-switched Nd:YAG nanosecond laser manufactured by BM Industries (model BMI 502 DNS 77/10), delivering 7 ns pulses at 1064 nm. The output energy was fixed at 5 mJ at 355 nm. The excitation beam and the probe beam generated by a pulsed xenon source were perpendicular to each other inside the 1 × 1 cm cell. The analysing beam was spectrally dispersed by a monochromator and converted to an electric signal by a Hamamatsu R928 PM tube. The electric signal was recorded by a digital memory oscilloscope (Tektronix TDS 654C) connected to a PC computer. Benzophenone triplet-state absorption in toluene solution was used as a standard for the determination of extinction coefficient of triplet states of ruthenium complexes.

Optical power limiting measurements

OPL curves were recorded from 730 nm to 990 nm using a Coherent Infinity XPO optical parametric oscillator (OPO) in the idler resonant mode (pump wavelength: 355 nm). The laser beam (pulse duration: 3 ns) was split in two parts, one used as reference beam and the other focused on the sample via a 120 mm focal length lens. Incident and transmitted energies were recorded using Laser Precision Rjp-765 silicon probes. For these experiments, complexes were dissolved at 50 g L^{-1} in chloroform, in 1-mm path-length cells.

III. Results and discussion

III.1. Synthesis

The synthesis of the new **PTFTF** ligand involving a triple bond connecting the two fluorene units (F) and one of these fluorenes to the polypyridyl moiety (1,10-phenanthroline, P), has been achieved by using a copper-free, palladium-catalyzed Sonogashira reaction[31,32] between 5-bromo-1,10-phenanthroline[33] and the difluorene derivative **4**. The latter was obtained via a Sonogashira cross-coupling reaction between the corresponding brominated derivative **3** and the trimethysilylane mono-protected actylene. This step was followed by a deprotection using potassium carbonate, leading to the terminal alkyne. Compound **3**, was also prepared according to a Sonogashira cross-coupling reaction starting from previously described **1** and **2** derivatives.[25,26] The **PTFTF:Ru** complex was obtained by reaction under reflux of three equivalents of the ligand with one equivalent of ruthenium trichloride (in dimethylformamide) and precipitated by saturated NH$_4$PF$_6$ solution. Compounds were fully characterized by NMR, high resolution mass, and elemental analysis.
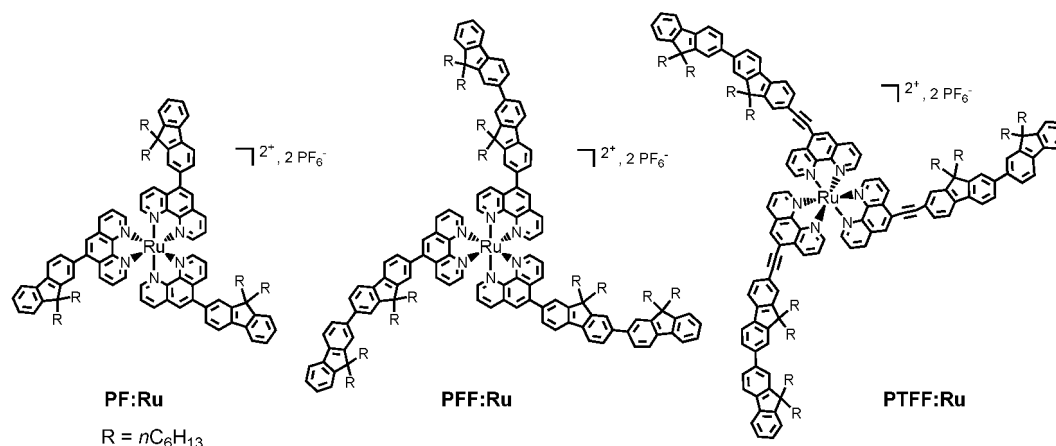

Fig. 3 Molecular structure of the **PF:Ru**, **PTFTF:Ru**, and **PTFTF:Ru** complexes.

III.2. Electronic spectroscopy of PTFTF and PTFTF:Ru

As previously observed for the complexes **PF:Ru**,[20] **PFF:Ru**,[20] and **PTFF:Ru**[24] (whose structures are reminded in Fig. 3, for convenience), the absorption spectrum of **PTFTF:Ru** exhibits three main groups of electronic transitions.

The absorption spectrum is composed of (a) a broad band in the 400–600 nm range, which corresponds to $d_\pi(Ru^{II}) \rightarrow \pi^*$-metal-to-ligand charge-transfer (MLCT) transitions and which is characteristic of this kind of Ru(II) complexes involving polypyridyle ligands, (b) a broad and very intense band between 330 and 420 m (λ_{max} around 400 nm), which, according to the theoretical results obtained for the free **PTFTF** ligand (see Table S4 in the ESI), is due to an intra-ligand charge-transfer (ILCT) transition involving a charge flow from the **TFTF** to the **PTF** moiety of the ligand. As shown in Fig. 4–a, this band is observed at nearly the same wavelengths as for the free **PTFTF** ligand ($\lambda_{max} = 380$ nm). In both cases, the large width of this absorption band can be mainly ascribed to the thermal and vibronic broadenings;[34] (c) finally, there is a third band around 270 nm which is mainly ascribed to π–π^* electronic transitions which are centered on aromatic ring such as the 1,10-phenanthroline moiety and the fluorene unit, or which corresponds to ILCT transitions of higher energies. This last absorption band and the ILCT one are similar to those observed in the **PTFF** and **PFF** ligand (see Fig. S2 and computational results of Tables S2 and S3 in the ESI).

Note that, for the theoretical characterization of the **PFF**, **PTFF**, and **PTFTF** ligands in the gas phase, we have used
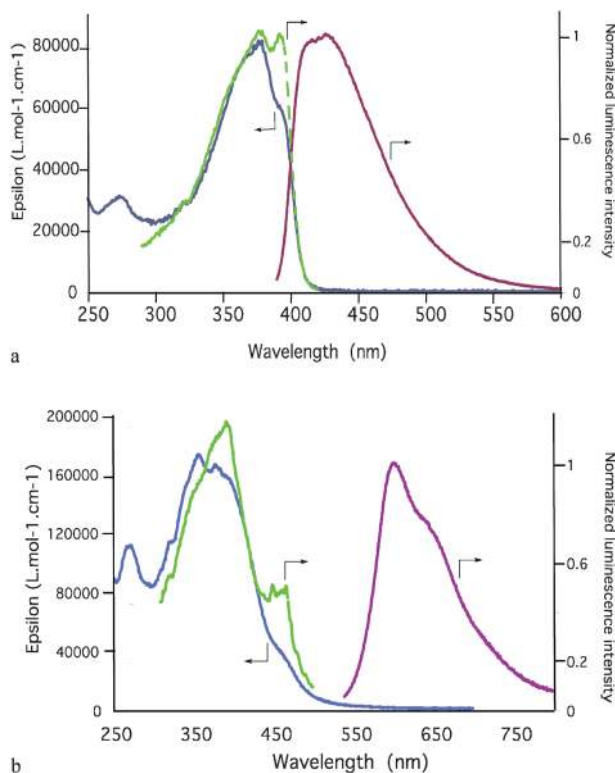

a

b

Fig. 4 Absorption (in chloroform), excitation (dotted line, in dichloromethane) and normalised emission spectra (in dichloromethane) of **PTFTF** (a) and the related **PTFTF:Ru** complex (b).

models obtained by replacing the n-hexyl chains of the ligands by hydrogen atoms (see ESI). The results of the geometry optimisation performed on these models indicate that, upon the insertion of the acetylenic fragment (T), one goes from nonplanar **PF** and **FF** moieties to planar **PTFF** and **FTF** moieties (Table S1, in ESI). The extent of the π-delocalisation thus increases on going from the **PFF** to the **PTFF** ligand and then to the **PTFTF** ligand; it is predicted to be accompanied with a redshift and an increase of the intensity of the low-energy CT transition (Tables S2–S4 in ESI). This is in satisfactory agreement with experiment.

Luminescence is observed for both the ligand and its Ru(II) complex in solution and at room temperature. Given that its decay-time is in the range of the μs for the complexes and of a few ns for the ligands (Table 1), the emission spectra observed for the complexes can be ascribed to the luminescence from the ^{3}MLCT state. The emission spectra of the **PTFTF** and the **PTFTF:Ru** are shown in Fig. 4–a and 4–b, respectively. A major difference between **PTFF:Ru**[24] (see Fig. 3 for reminding the molecular structure) and the novel **PTFTF:Ru** complex, is the increased intensity of the ILCT band due to the increased extent of the π-coupling (see above). The influence of the ligand structure is also evidenced in the increase of the quantum yield and excited state lifetime (5% and 2.7 μs, compared to 2% and 0.71 μs for **PTFTF:Ru** and **PTFF:Ru**, respectively). These results are in good agreement with the corresponding radiative and non-radiative decay rate constants (k_r and k_{nr}, respectively, in 10^6 s^{-1}).

The influence of the solvent on the room-temperature luminescence properties of the ligand PTFTF has also been investigated. The luminescence spectra (displayed in Fig. 5) consist in broad bands centered at 400, 426 and 435 nm in hexane, CH$_3$CN and DMSO, respectively. Maximum absorption and emission wavelengths, Stokes shifts, quantum yields and excited state lifetimes of all discussed compounds are reported in Table 1. The lifetime decay of these organic compounds in deoxygenated CH$_3$CN solution, recorded at 480 nm after excitation at 400 nm, are all mono-exponential. The emission decay times τ (see Table 1) of about a few nanoseconds are in good agreement with a singlet excited state emission. A structured emission spectrum is observed for PTFTF in hexane and diethyl ether. The mean vibrational spacing is around 1500 cm^{-1} which corresponds to aromatic $\nu_{C=C}$ elongation modes.

The Stokes shift determined for the ligand **PTFTF** has been plotted against the solvent Dimroth-Reichardt E_T^N parameter.[36] This plot is shown in Fig. 6 along with the plot similarly made for the **PFF** ligand. The relationship between the Stokes shift and the solvent polarity is usually given by the Lippert-Mataga equation.[37,38] This correlation (see eqn (2)) is the most widely used equation to describe the effects of the physical properties of the solvent on the emission spectra of fluorophores. It has been used here, to estimate the variation ($\mu_{CT}-\mu_g$), in the dipole moment between the ground and the excited states (polarizability).

$$\Delta\nu_{ST} = \Delta\nu_{ST}^0 + \left[\frac{2}{(4\pi\varepsilon_0)(hca^3)}\right] \times (\mu_{CT} - \mu_g)^2 \times \Delta f(\varepsilon, n)$$

$$(2)$$

Table 1

Compound	λ_{abs} $(\varepsilon_{max})^a$	Attribution	$\lambda_{em}{}^b$	$\lambda_{exc}{}^c$	$\phi_L{}^d$	τ^e	$k_r{}^f$	$k_{nr}{}^f$
PFF[20]	272 (30500)	$\pi-\pi^*$ phen	427	278	0.9	1.6	—	—
	365 (68300)	CT		375				
PTFF[24]	272 (30500)	$\pi-\pi^*$ phen	427	278	0.9	1.6	—	—
	365 (68300)	CT		375				
PTFTF	275 (30600)	$\pi-\pi^*$ phen	427		0.8	1.1	—	—
	377 (80500)	CT		377				
	392 (sh. 59500)	CT		392				
PTFF:Ru[24]	275 (97400)	IL phen	596		0.02	708	280	1.4
	340 (142700)	ILCT		350 (sh.)				
	400 (104400)	ILCT + MLCT		398				
	450 (sh.)	MLCT		456				
PTFTF:Ru	271 (110100)	IL phen	601		0.05	2700	190	0.4
	378 (164900)	ILCT + MLCT		393				
	460 (sh.)	MLCT		458				

^{a} Maximum linear absorption in nm (molecular absorption coefficients at λ_{max} in L mol^{-1} cm^{-1}) in chloroform. ^{b} Maximum emission in nm in dichloromethane. ^{c} λ_{exc} Maximum of the excitation spectra in nm. ^{d} ϕ_L luminescence quantum yield in CH$_2$Cl$_2$ using p-bis(o-methylstyryl)-benzene as reference (MSB). $\phi_L^{ref} = 1)^{35}$ and in deoxygenated CH$_2$Cl$_2$ using Ru(bipy)$_3^{2+}$ ($\phi^{ref} = 0.062)^{34}$ as reference for ligands and Ru(II) complexes, respectively. ^{e} τ: luminescence lifetime measured in ns in CH$_3$CN. (sh.:shoulder). ^{f} k_r and k_{nr}: radiative and non-radiative decay constants in 10^6 s^{-1}.
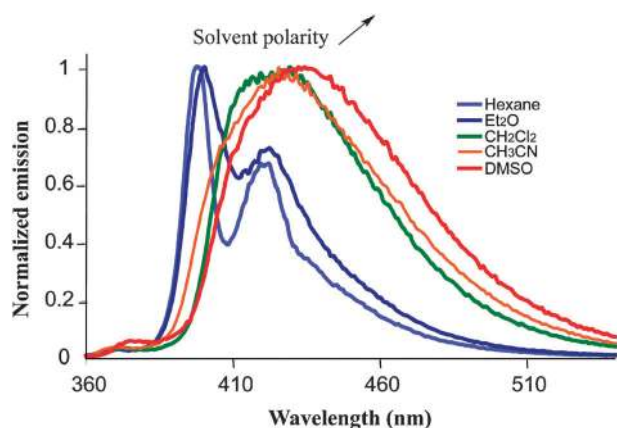

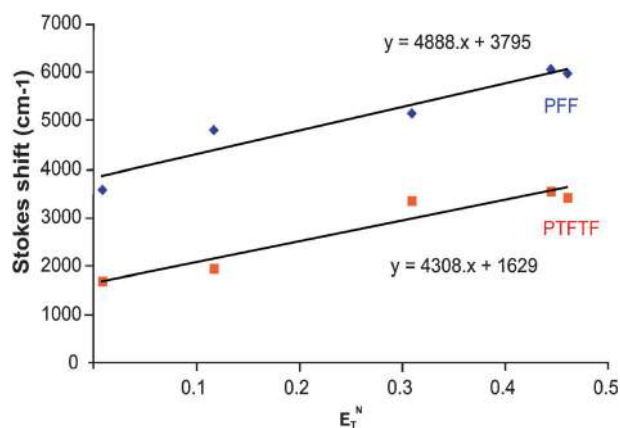**Fig. 5** Emission spectra of the **PTFTF** ligand in a series of solvents.

Fig. 6 (a) Plot of Stokes shift ($\Delta\nu_{ST}$) against Dimroth-Reichardt E_T^N parameter (see Table 2) and correlation according to eqn (2) of the Stokes shift and the Lippert-Mataga polarity parameter for compounds **PFF** and **PTFTF** in the five solvents listed in Table 1 ($R^2 = 0.93$ for both compounds).

where a is the value of the Onsager cavity radius in which the fluorophore resides, h is the Planck's constant, c is the speed of light, ε_0 is the vacuum permittivity and $\Delta f(\varepsilon,n)$ is the orientational polarizability defined as:

$$\Delta f(\varepsilon,n) = \frac{\varepsilon - 1}{2\varepsilon + 1} - \frac{n^2 - 1}{2n^2 + 1} \qquad (3)$$

where ε is the static dielectric constant and n, the refractive index of the solvent.

For both ligands, the plots are found to be linear with a correlation factor $R^2 = 0.93$. This suggests that dipole–dipole interactions between the solute and the solvent are mainly responsible for the solvent-dependent fluorescence shift.

The slope (proportional to $[\mu_{CT}-\mu_g]^2/a^3$ according to eqn (2)) is 1.13 larger for the **PFF** compound than for the **PTFTF** one. This indicates that the polarizability should be quite similar for **PTFTF** and **PFF**. Actually, using the Onsager radius estimates of 5.8 and 6.0 Å calculated for **PFF** and **PTFFF**, respectively (see ESI), we have $(\mu_{CT}-\mu_g)_{\textbf{PTFTF}} = 0.99 (\mu_{CT}-\mu_g)_{\textbf{PFF}}$. Therefore, and as recently reported in the literature,[39] a similar efficiency in nonlinear optics may also be expected for the **PTFTF** and **PFF** compounds.

III.3. Two-photon absorption spectrum of PTFTF and PTFTF:Ru

Two-photon absorption cross-section σ_{TPA} of the **PTFTF** ligand has been measured between 700 and 850 nm (Fig. 7 and Table 3). The value at 700 nm (40.10^{-50} cm^4 s photon^{-1}, 40 G.M.) can be compared to the value obtained for the **PFF** ligand (around 20 G.M.). This comparison depends on the wavelength, but it confirms that there is no significant increase of the TPA cross-section on going from the **PFF** to the **PTFTF** compound.

The **PTFTF:Ru** complex involving this conjugated ligand presents a larger and red-shifted σ_{TPA} value than the previously described **PTFF:Ru** for optical power limiting application (around 350 and 250 G.M. between 750 and 850 nm); see Table 1 and Fig. 8.
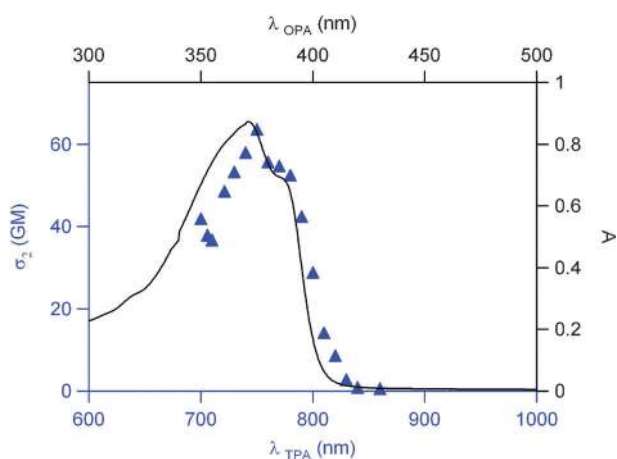
Fig. 7 Two-photon excitation spectrum of **PTFTF** measured in acetonitrile (the experimental uncertainty is ± 15%). For comparison, linear excitation spectrum of this ligand was also reported.

III.4. Transient absorption spectrum

ESA (see Fig. 8) is attributed to triplet–triplet absorption of ^{3}MLCT excited states of Ru^{2+} tris-chelate complexes.[40] The decay times of these transient absorption signals are in the microsecond range in agreement with the luminescence lifetimes (see Table 1). A longer luminescence lifetime of 2.7 µs for **PTFTF:Ru** with respect to 0.7 µs for **PTFF:Ru** is observed; this may be attributed to the highest conjugation of the **PTFTF** ligand leading to a less efficient non-radiative process (k_{nr} = 1.4 and 0.4 s^{-1} for **PTFF:Ru** and **PTFTF:Ru**, respectively). Similar ESA properties were obtained in the two complexes with an extinction coefficient ε_{ESA} of around 9500 M^{-1} cm^{-1} at 840 nm (Fig. 8 and Table 1) nevertheless, the ESA spectrum is slightly red-shifted for the complex, **PTFTF:Ru** again in agreement with the more conjugated nature of this ligand. As far as the spectral overlap between TPA and ESA processes required for an optimised nonlinear absorption (Fig. 8) is concerned, it should be pointed that in **PTFTF:Ru**, high σ_{TPA} values are observed between 700 and 900 nm (500 to 50 GM with a maximum around 380 GM at 810 nm), while efficient ESA absorption is detected and measured in the range 750–900 nm. As for **PTFF:Ru**, and more than in the **PFF:Ru** compound, it leads to a broad overlap between both spectra in the 750–900 nm region.

III.5. Optical power limiting

III.5.1. Nonlinear transmission. Here, we inspect the global phenomenon based on the two-photon absorption and excited state absorption of a third photon. As shown by the nonlinear transmission curves plotted in Fig. 9, the **PTFTF:Ru** complex

Table 2 Relative permittivity (ε) at 25 °C, refractive index (n) and Reichardt's E_T values of solvents

Solvents	$\varepsilon^{25°}$	$n_D^{20°}$	E_T^N
Cyclohexane	2.0	1.426	0.006
Diethyl-ether	4.2	1.353	0.117
Dichloromethane	8.9	1.424	0.309
CH$_3$CN	35.9	1.344	0.460
DMSO	46.4	1.479	0.444

Table 3

Compound	λ_{TPA}[a] (σ_{TPA})	λ_{ESA}[b] (σ_{ESA})	Ref
PFF	560 (80)	—	20
	700 (20)		
PTFF	600 (250)	—	25
PTFTF	700 (40)	—	This work
	760 (65)		
PFF:Ru	850 (15)	830 (2700)	20
PTFF:Ru	800 (15)	820 (9500)	24
	870 (40)		
PTFTF:Ru	700 (530)	840 (9500)	This work
	820 (390)		
	880 (100)		

[a] Maximum TPA wavelength in nm, in acetonitrile (TPA cross-section in GM stands for Göppert-Mayer with 1 GM = 10^{-50} cm^4 s photon^{-1}). [b] Maximum wavelength ESA in nm in acetonitrile (ESA extinction coefficient in M^{-1} cm^{-1}).
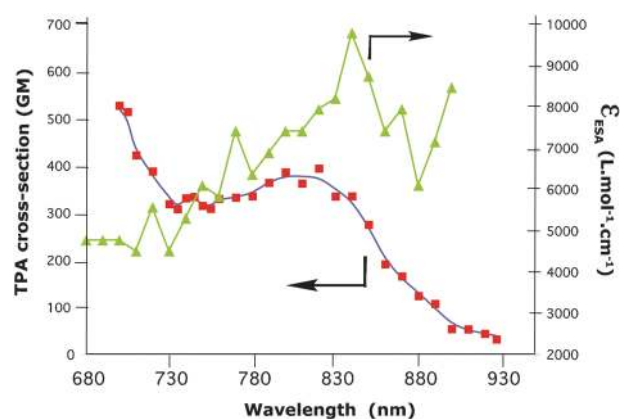

Fig. 8 TPA and ESA spectra of **PTFTF:Ru** in chloroform (the experimental uncertainty is ± 15%); figure represents ESA coefficients experimental points; lines are given for clarity of the lecture.
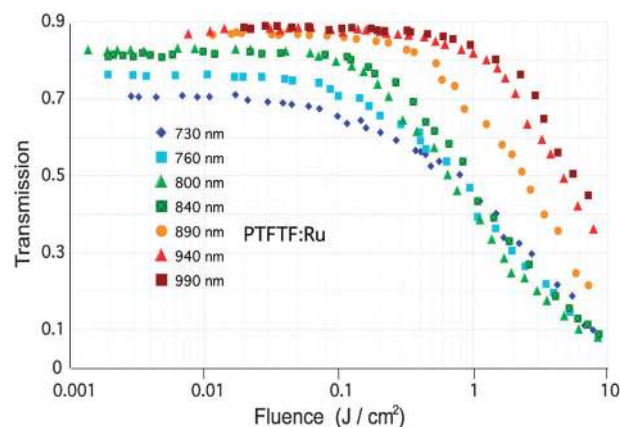

Fig. 9 Nonlinear transmission curves in chloroform between 730 and 990 nm of **PTFTF:Ru** complex at 50 g l^{-1}.

presents typical broad-band OPL properties between 730 and 990 nm. In the 800–900 nm range, the initial linear transmission at low fluences (80 to 85%) shows the absence of the contribution of a reverse saturable absorption process to the nonlinear transmission. The decrease of the transmission for higher energy
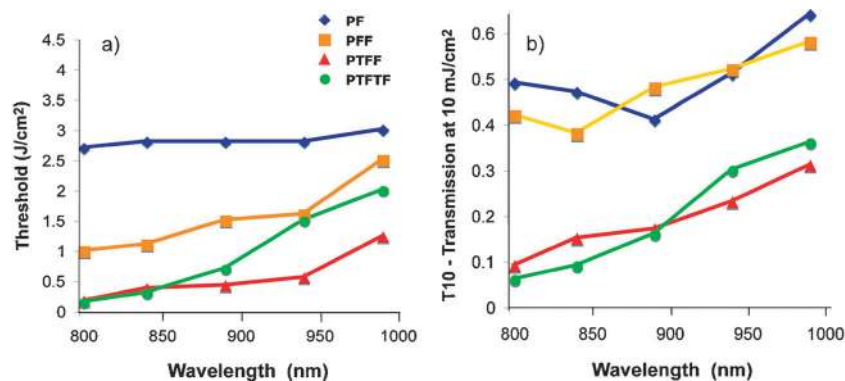
Fig. 10 Th(a) and T_{10} (b) variations between 800 and 990 nm for **PTFTF:Ru**, **PTFF:Ru**, **PFF:Ru**, and **PF:Ru** complexes at 50 g L^{-1} (figures represent experimental points and lines are given for clarity of the lecture).

Table 4 Optical limiting data for complexes **PTFTF:Ru**, **PTFF:Ru**, and **PFF:Ru** in chloroform at 50 g l^{-1}

	$Th^{750}(Th^{900})^a$	$T_{10}^{750}(T_{10}^{900})^b$
PTFTF:Ru	0.4 (0.8)	0.08 (0.15)
PTFF:Ru	0.2 (0.3)	0.11 (0.15)
PFF:Ru	0.6 (1.5)	0.28 (0.48)

^{a} Th (in J cm^{-2}) is the OPL threshold at 750 nm (Th^{760}) and 900 nm (Th^{900}); the threshold was determined graphically as the intersection between the linear and the nonlinear part of the OPL curve.[39] ^{b} $T_{10}^{750}(T_{10}^{900})$ is the transmittance for an incident fluence of 10 J cm^{-2} at 750 (900 nm).

photons (wavelength between 730 and 800 nm), can ascribed to a weak residual linear absorption at these wavelengths.

The dependences on the laser wavelength (800–990 nm) of the optical limiting threshold Th and of the transmittance T_{10} are reported in Fig. 10 for all the complexes of the family at an incident fluence of 10 J cm^{-2}, and in comparison with σ_{TPA}. The spectral dispersion of Th and T_{10} shows a similar efficiency at all wavelength of the more conjugated complexes **PTFTF:Ru** and **PTFF:Ru**, for which both parameters are reported in Table 4. These parameters are significantly smaller (revealing a higher efficiency) than those of the two other complexes of the family (**PF:Ru** and **PFF:Ru**, see Fig. 3 for the structure of these ligands). For the **PTFTF:Ru** and **PTF:Ru** complexes, the T_{10} and Th curves both present a minimum around 800 nm, that is at the same wavelength as the maximum of the σ_{TPA} curve. This wavelength does not correspond to the maximum of the σ_{ESA}, nevertheless excited state absorption is still quite large at this wavelength (7000 L. mol^{-1} cm^{-1} for a maximum absorption coefficient of 9000 L mol^{-1} cm^{-1}) and the overlap between the TPA and ESA spectra is broad over the consider wavelength range. This trend confirms the role of both the TPA and ESA phenomena in TPA based OPL processes. The threshold values measured for **PTFTF:Ru** and **PTFF:Ru** are of the same order of magnitude as those measured for organic systems[41] but with a broader wavelength range of efficiency in our case.

IV. Conclusion

We designed a novel fluorene-substituted 1,10-phenanthroline based Ru(II) coordination complex **PTFTF:Ru**, which fulfill

several requirements for optimized OPL in the near infra-red (NIR): synthesis accessibility in few hundreds of milligrams scale, excellent stability, high solubility compatible with OPL studies in organic solvents and relative good transparency at low laser fluences. This complex exhibits TPA properties in intraligand as well as in the MLCT bands between 700 and 900 nm. These properties, were shown to be strongly related to those of the ligand (which has been more theoretically analyzed). A broad spectral overlap between TPA an ESA was obtained for the complex. This leads to promising broad-band OPL properties in the NIR for this complex, for which a quite high ESA cross-section is in good agreement with efficiencies above 850 nm.

References

1 C. W. Spangler, *J. Mater. Chem.*, 1999, **9**, 2013–2020.
2 X. Sun, R. Q. Yu, G. Q. Xu, T. S. A. Hor and W. Ji, *Appl. Phys. Lett.*, 1998, **73**, 3632–3634.
3 L. Vivien, E. Anglaret, D. Riehl, F. Bacou, C. Journet, C. Goze, M. Andrieux, M. Brunet, F. Lafonta, P. Bernier and F. Hache, *Chem. Phys. Lett.*, 1999, **307**, 317–319.
4 B. Dupuis, C. Michaut, I. Jouanin, J. Delaire, P. Robin, P. Feneyrou and V. Dentan, *Chem. Phys. Lett.*, 1999, **300**, 169–176.
5 G.-J. Zhou, W.-Y. Wong, Z. Lin and C. Ye, *Angew. Chem., Int. Ed.*, 2006, **45**, 6189–6193.
6 G.-J. Zhou, W.-Y. Wong, C. Ye and Z. Lin, *Adv. Funct. Mater.*, 2007, **17**, 963–975.
7 S. Shettigar, G. Umesh, K. Chandrasekharan and B. Kalluraya, *Synth. Met.*, 2007, **157**, 142–146.
8 G. S. He, G. C. Xu, P. N. Prasad, B. A. Reinhardt, J. C. Bhatt and A. G. Dillard, *Opt. Lett.*, 1995, **20**, 435–437.
9 J. E. Ehrlich, X. L. Wu, I.-Y. S. Lee, Z.-Y. Hu, H. Röckel, S. R. Marder and J. W. Perry, *Opt. Lett.*, 1997, **22**, 1843–1845.
10 R. Anémian, Y. Morel, P. L. Baldeck, B. Paci, K. Kretsch, J.-M. Nunzi and C. Andraud, *J. Mater. Chem.*, 2003, **13**, 2157–2163.
11 M. Charlot, N. Izard, O. Mongin, D. Riehl and M. Blanchard-Desce, *Chem. Phys. Lett.*, 2006, **417**, 297–302.
12 P.-A. Bouit, G. Wetzel, G. Berginc, B. Loiseaux, L. Toupet, P. Feneyrou, Y. Bretonnière, K. Kamada, O. Maury and C. Andraud, *Chem. Mater.*, 2007, **19**, 5325–5335.
13 T.-C. Lin, Y.-J. Huang, Y.-F. Chen and C.-L. Hu, *Tetrahedron*, 2010, **66**, 1375–1382.
14 R. Vestberg, R. Westlund, A. Eriksson, C. Lopes, M. Carlsson, B. Eliasson, E. Glimsdal, M. Lindgren and E. Malmstrom, *Macromolecules*, 2006, **39**, 2238–2246.
15 E. Glimsdal, M. Carlsson, B. Eliasson, B. Minaev and M. Lindgren, *J. Phys. Chem. A*, 2007, **111**, 244–250.

16 S. K. Hurst, M. G. Humphrey, J. P Morrall, M. P. Cifuentes, M. Samoc, B. Luther-Davis, G. A. Heath and A. C. Willis, *J. Organomet. Chem.*, 2003, **670**, 56–65.

17 B. J. Coe, M. Samoc, A. Samoc, L. Zhu, Y. Yi and Z. Shuai, *J. Phys. Chem. A*, 2007, **111**, 472–478.

18 C. Feuvrie, O. Maury, H. Le Bozec, I. Ledoux, J. P. Morrall, G. T. Dalton, M. Samoc and M. G. Humphrey, *J. Phys.Chem. A*, 2007, **111**, 8980–8985.

19 M. Samoc, J. P. Morrall, G. T. Dalton, M. P. Cifuentes and M. G. Humphrey, *Angew. Chem., Int. Ed.*, 2007, **46**, 731–733.

20 C. Girardot, G. Lemercier, J.-C. Mulatier, J. Chauvin, P. L. Baldeck and C. Andraud, *Dalton Trans.*, 2007, 3421–3426.

21 M. G. Humphrey, B. Lockhart-Gillet, M. Samoc, B. W. Skelton, V.-A. Tolhurst, A. H. White, A. J. Wilson and B. F. Yates, *J. Organomet. Chem.*, 2005, **690**, 1487–1497.

22 C. E. Powell, M. P. Cifuentes, M. G. Humphrey, A. C. Willis, J. P. Morrall and M. Samoc, *Polyhedron*, 2007, **26**, 284–289.

23 T. V. Duncan, P. R. Frail, I. R. Miloradovic and M. J. Therien, *J. Phys. Chem. B*, 2010, **114**, 14696–14702.

24 C. Girardot, B. Cao, J.-C. Mulatier, P. L. Baldeck, J. Chauvin, D. Riehl, J. A. Delaire, C. Andraud and G. Lemercier, *ChemPhysChem*, 2008, **9**, 1531–1535.

25 C. Girardot, G. Lemercier, J.-C. Mulatier, C. Andraud, J. Chauvin and P. L. Baldeck, *Tetrahedron Lett.*, 2008, **49**, 1753–1758.

26 R. Kannan, G. S. He, T. C. Lin, P. N. Prasad, R. A. Vaia and L. S. Tan, *Chem. Mater.*, 2004, **16**, 185–194.

27 C. Xu and W. W. Webb, *J. Opt. Soc. Am. B*, 1996, **13**, 481–491.

28 M. H. V. Werts, N. Nerambourg, D. Pélégry, Y. Le Grand and M. Blanchard-Desce, *Photochem. Photobiol. Sci.*, 2005, **4**, 531–538.

29 C. Katan, S. Tretiak, M. H. V. Werts, A. J. Bain, R. J. Marsh, N. Leonczek, N. Nicolaou, E. Badaeva, O. Mongin and M. Blanchard-Desce, *J. Phys. Chem. B*, 2007, **111**, 9468–9483.

30 J. Zakrzewski, J. A. Delaire, C. Daniel and I. Cote-Bruand, *New J. Chem.*, 2004, **28**, 1514–8.

31 A. Tougerti, S. Negri and A. Jutand, *Chem.–Eur. J.*, 2007, **13**, 666–676.

32 G. T. Crisp and J. Gore, *Tetrahedron*, 1997, **53**, 1505–1522.

33 M. Hissler, W. B. Connick, D. K. Geiger, J. E. McGarrah, D. Lipa, R. J. Lachicotte and R. Eisenberg, *Inorg. Chem.*, 2000, **39**, 447–457.

34 L. M. Lawson-Daku, J. Linares and M.-L. Boillot, *Phys. Chem. Chem. Phys.*, 2010, **12**, 6107–6123.

35 J. Sujatha and A. K. Mishra, *J. Photochem. Photobiol., A*, 1996, **101**, 245–250.

36 C. Reichardt, *Chem. Rev.*, 1994, **94**, 2319–2358.

37 N. Mataga, *Bull. Chem. Soc. Jpn.*, 1963, **36**, 654–659.

38 J. R. Lakowicz, *Principles of Fluorescence Spectroscopy*, Plenum Press, New York, 1983.

39 F. Terenziani, C. Le Droumaguet, C. Katan, O. Mongin and M. Blanchard-Desce, *ChemPhysChem*, 2007, **8**, 723–734.

40 X.-Y. Wang, A. Del Guerzo and R. H. Schmehl, *J. Photochem. Photobiol., C*, 2004, **5**, 55–77.

41 M. G. Silly, L. Porrès, O. Mongin, P.-A. Chollet and M. Blanchard-Desce, *Chem. Phys. Lett.*, 2003, **379**, 74–80.